Hyperlocal Spatial Flows in BOLD fMRI Expose Novel Brain-Based Correlates of Schizophrenia

Robyn L. Miller^{1*}, Victor M. Vergara¹ and Vince D. Calhoun¹

¹The Tri-Institutional Center for Translational Research in Neuroimaging and Data Science (TReNDS Center): Georgia State University, Georgia Institute of Technology and Emory University, Atlanta, GA USA

ABSTRACT

While analysis of temporal signal fluctuations has long been a fixture of blood oxygenation-level dependent (BOLD) functional magnetic resonance imaging (fMRI) research, the role of spatially localized directional diffusion in both signal propagation and emergent large-scale functional integration remains almost entirely neglected. We are proposing an extensible framework to capture and analyze spatially localized fMRI directional signal flow dynamics. The approach is validated in a large resting-state fMRI schizophrenia study where it uncovers significant and novel relationships between hyperlocal spatial dynamics and subject diagnostic status.

1. INTRODUCTION

The patterns of activated brain space measured by BOLD fMRI are typically investigated via pairwise correlations between timeseries corresponding to a fixed collection of functionally-identifiable brain regions or distributed networks [1-3]. This reduced representation of the BOLD signal is referred to static functional network connectivity (sFNC) when the entire scan-length timeseries are employed and dynamic functional network connectivity (dFNC) when the correlations are evaluated on successive shorter sliding windows through the scan. Dynamic functional network connectivity can capture large scale patterns of brainwide coactivation that change with time, but entirely neglects the role of localized spatial signal flows in producing - or, in various clinical disorders, impeding - familiar large-scale patterns of resting-state functional integration. Our understanding of the brain based on fMRI is still limited by a critical information gap between standard connectivity-based analyses and the processes of activation propagation through chains of voxel-scale neuronal populations that underpin such high-level imaging measures.

2. METHODS

2.1 Data

We use data from a large, eyes-closed resting-state functional magnetic resonance imaging (fMRI) study with approximately equal numbers of schizophrenia patients (SZs) and healthy controls (HCs) (n=314, nSZ=151). Scans were preprocessed according to a standard, previously published pipeline [4], with an additional stage of spatial and temporal smoothing to control noise in the estimated spatial derivatives. This extra processing consisted of smoothing preprocessed scans with a 3D Gaussian kernel (σ = 3) and 1D temporal moving average with windows of length 3. The gray matter mask for this data contained 60303 voxels: the x-

dimension (coronal) has length 53; the y-dimension (sagittal) has length 63; the z-dimension (axial) has length 46. There are 158 sampled timepoints in each scan. All subjects in the study signed informed consent forms.

2.2 Group ICA on Scan Data

As described in previously published work [4] the scan data for this study was decomposed with group independent component analysis (GICA) into 100 group-level functional network spatial maps (SMs) and corresponding subject-specific timecourses (TCs).



Figure 1 Condensed schematic for group ICA (top) and the components identified in this data from previous work (bottom)

Through a combination of automated and manual pruning, N=47 functional networks were retained (see Figure 1).

2.3 Spatiotemporal Gradients (STGs)

To diminish confounding of spatiotemporal gradients by subject differences in global signal amplitude, each preprocessed fMRI volume is rescaled by its own mean amplitude. For each voxel $v=(x,y,z)\in\mathbb{R}^{53\times63\times46}$ and each TR $t\in\{1,2,...,158\}$ in an fMRI volume, let F(v,t)=F(x,y,z,t) denote the amplitude-normalized fMRI signal at (x,y,z,t). At every voxel and timepoint, we now consider $\nabla_t F(v,t) = \frac{\partial}{\partial t} \left(f_x(x,y,z,t), f_y(x,y,z,t), f_z(x,y,z,t) \right)$ where: $f_x = dF/dx$, $f_y = dF/dy$ and $f_z = dF/dz$. The numerical directional and space-time derivatives are computed via the central difference method, e.g., $f_x(x,y,z,t) = \frac{1}{2}(F(x+1,y,z,t) - F(x-1,y,z,t))$ and $\frac{\partial}{\partial t} f_x(x,y,z,t) = \frac{1}{2}(f_x(x,y,z,t+1) - f_x(x,y,z,t-1))$. This yields three new volumes $F_x = \frac{\partial}{\partial t} f_x$, $F_y = \frac{\partial}{\partial t} f_y$ and $F_z = \frac{\partial}{\partial t} f_z$, each of the same dimensionality as F.

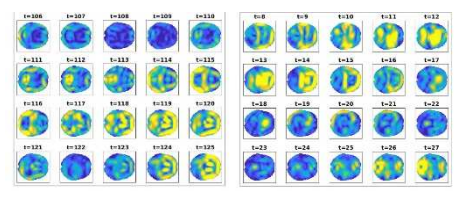


Figure 2 Examples of evolving SPF in a single axial slice over two disjoint 20TR intervals: $t \in [106,125]$ (left) and $t \in [8,27]$ (right)

2.4 Voxel-Localized Spatially Propagative Force (SPF)

As a first-pass dimensionreduction step, we define the scalar-valued spatiotemporal propagative force (SPF) (see **Figure 2**) at each voxel and timepoint as the non-negative directionless summary measure $\widehat{F}(v,t) \equiv \max_{\theta \in \{x,y,z\}} (|F_{\theta}(v,t)|)$, the largest magnitude spatiotemporal derivative at each (v,t).

2.5 Group ICA on SPFs

In addition to the group ICA performed on preprocessed scan data, we also use group ICA (model order 50) to identify spatially independent components representing the spatially propagative force measure described above. SPF GICA spatial maps present mutually independent patterns of high-intensity voxels that exhibit highly temporally coherent SPF behavior (see Figure 3).

2.6 Hybrid Spatiofunctional Dynamic Connectivity (SFdC) and Clustering

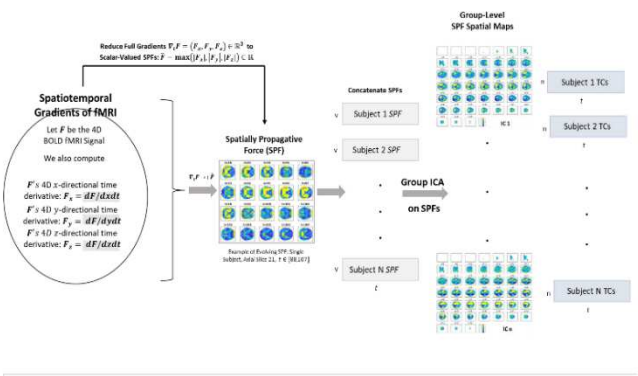




Figure 4 Pipeline for creating components and timecourses representing SPF patterns in the brain: 1. Compute numerical spatiotemporal gradients; 2. Convert 3D gradients to scalar-valued SPF measures, i.e., maximum magnitude among the three directional derivatives; 3. Group ICA on SPFs; (Bottom) Sample SPF spatial maps.

Following the paradigm typically applied to GICA FN timecourses for now-standard dynamic functional network (dFNC) analysis [5-8], we consider windowed correlations between all timecourses from both the SPF and FN GICAs. These are measures of global functional integration (FN-FN) contextualized by the concurrent patterns of localized spatial propagation strength. Familiar dFNC patterns (Figure 12, [4]) can manifest under different background conditions in patterned local spatial propagation, potentially highlighting group differences in measurable brain dynamics that support or predict commonly reported transient states of functional integration, i.e. dFNC.

Correlations are computed on rectangular sliding windows of length 22TRs, advancing 1 TR at a time with the windowlength selected based on previous work [4]. The resulting set of nWins*nSubs vectors of length $\frac{(50+47)(50+46)}{(50+47)(50+46)} = 4656$ are then clustered, using the

correlation metric, with k-means into k = 10 spatiofunctional dynamic connectivity (SFdC) "states" (see **Figure 4**), with k

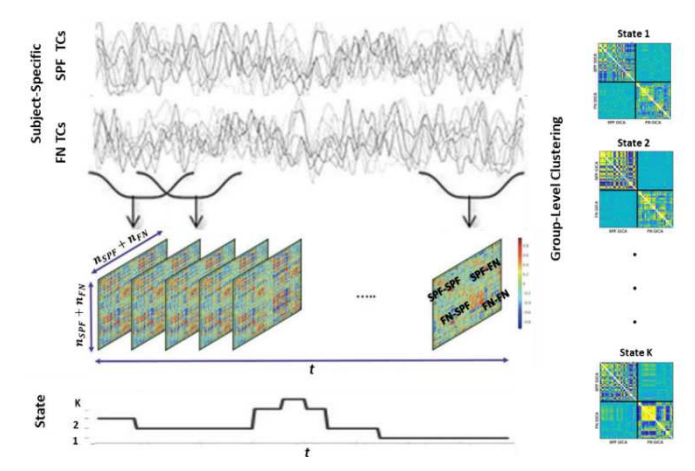


Figure 3 Dynamic hybrid connectivity pipeline: windowed pairwise correlations between all $n_{SPF} + n_{FN}$ component timeseries, followed by clustering and quantification of subject occupancy patterns.

selected using the elbow criterion.

2.7 Display Conventions

The 4page space constraint has made it difficult to retain readable figure text. In general, displays of the whole brain (e.g. **Figure 3** (bottom row), **Figure , Figure , Figure , Figure)** are shown as successive axial slices from z=1 (top left) to z=46 (bottom right). Displays of hybrid SPF-FN connectivity have SPF components first along each axis, followed by FN components. The bottom right block, more familiar FN connectivity is sometimes gridded with respect to network functional domain (subcortical (SC), auditory (AUD), visual (VIS), sensorimotor (SM), cognitive control (CC), default mode network (DMN), cerebellum (CB)). Color maps are fixed and symmetric about zero, except in cases where the measure itself, e.g., SPF (e.g. **Figure 2**), is nonnegative.

2.8 Statistical Analysis

The effects of SZ diagnosis reported here are obtained through a multiple regression model on SZ diagnosis, gender, age and motion. Displayed effects are significant (p < 0.05) after correction for multiple comparisons, unless otherwise indicated. Colormaps are symmetric about zero, with cooler (resp. warmer) colors indicating negative (resp. positive) SZ effects.

3. RESULTS

We present here a variety of preliminary results that paint a complex picture in which the local spatial flow strengths, both directional and directionless, average out in structured patterns that also carry structured effects of SZ (Figure 5, Figure 6, Figure 7, Figure 8, Figure 9). The group ICAs on SPFs and on preprocessed fMRIs produce very different representations of the brain. Group-level spatial maps in the two GICAs are negligibly spatially correlated (Figure 11 (middle)) and the subject-specific component timecourses from both ICAs also exhibit representations of the brain. Group-level spatial maps in the two GICAs are negligibly

spatially correlated (Figure 11 (middle)) and the subjectspecific component timecourses from both ICAs also exhibit negligible temporal correlations (Figure 11 (right)). Although the independent patterns of spatiotemporal flow strength, i.e., the SPF GICA component maps (examples in Figure 3 (bottom row)), and their temporal contributions to subject SPFs are not tractably related to FN GICA component maps or their temporal contributions to subject scan data, the two decompositions show evidence (Figure 10, Figure 13) of transient concurrencies that may distinguish the ways that different subjects and, e.g. conical groups, pass through dFNC states that are regularly reported upon. Group differences in dFNC trajectories may be partly driven by local spatially propagative "subprocesses" that aggregate to constrain or support the larger scale functional reorganization reflected in dFNCs. In particular the highly modularized dFNC state in which the auditory-visual-sensorimotor networks (AVSN) are tightly intercorrelated whilst simultaneously being strongly anticorrelated with cognitive control and default mode networks is realized in slightly different forms and against different SPF backgrounds in SZ patients and healthy controls (Figure 10, Figure 12, Figure 13)

3.1 Direction-Specific Spatiotemporal Derivative Magnitudes Present Structured Patterns Impacted by SZ

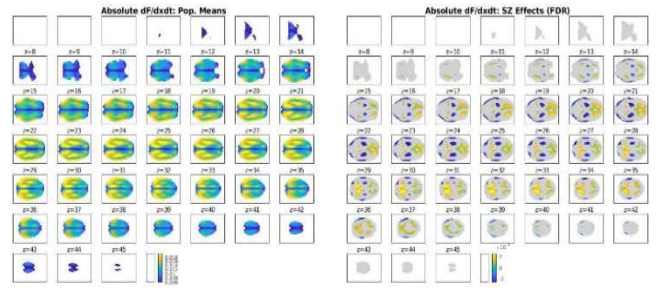


Figure 5 Coronal Direction: Absolute x-Derivative w.r.t time $(|F_x|)$. Population means (left) and significant SZ effects (right). Consult Sections 2.7 and 2.8 for details on display and statistical modeling.

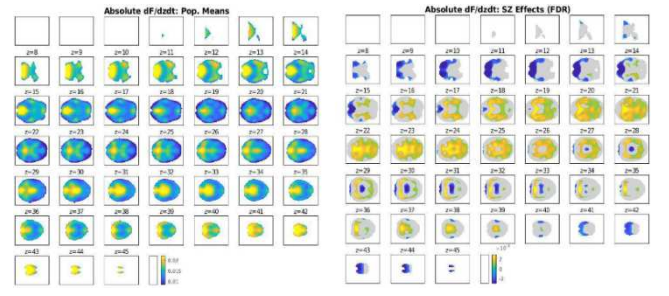


Figure 6 Sagittal Dimension: Absolute y-Derivative w.r.t time $(|F_y|)$. Population means (left) and significant SZ effects (right). Consult Sections 2.7 and 2.8 for details on display and statistical modeling.

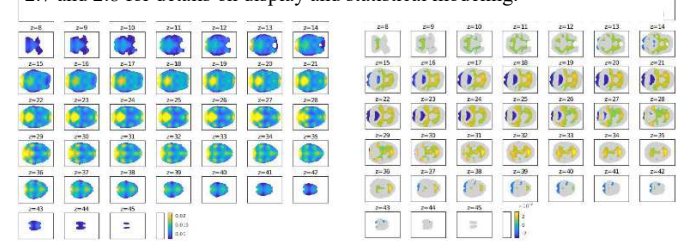


Figure 7 Axial Dimension: Absolute z-Derivative w.r.t time $(|F_z|)$. Population means (left) and significant SZ effects (right). Consult Sections 2.7 and 2.8 for details on display and statistical modeling.

3.2 Directionless Summaries of Spatiotemporal Derivative Magnitudes

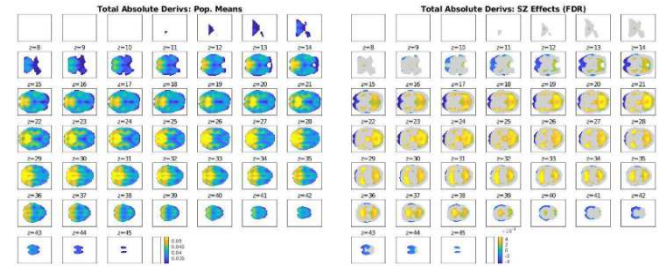


Figure 8 Sum of Absolute x,y and z-Derivatives w.r.t time $(|F_x| + |F_y| + |F_z|)$. Population means (left) and significant SZ effects (right). Consult Sections 2.7 and 2.8 for details on display

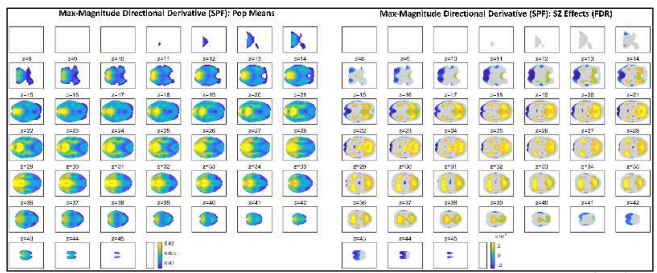


Figure 9 Max of Absolute x,y and z-Derivatives w.r.t time $(|F_x| + |F_y| + |F_z|)$, i.e. SPF Population means (left) and significant SZ effects (right). Consult Sections 2.7 and 2.8 for details on display and statistics. This is the measure that SPF group ICA is performed upon.

3.3 Hybrid Spatiofunctional Dynamic Connectivity States

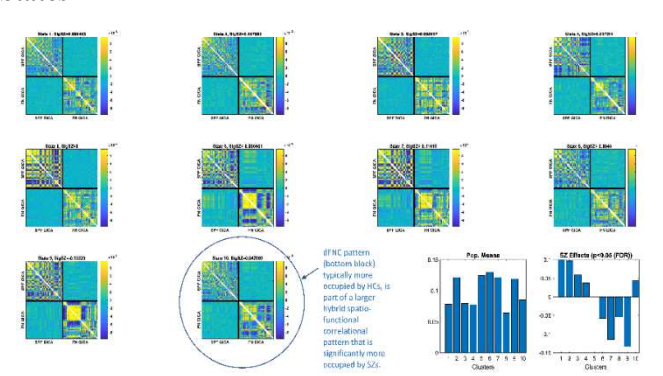


Figure 5 Hybrid Spatiofunctional Dynamic Connectivity States (SFdC) States. SPF-SPF in upper left block of each heatmap and FN-FN in the lower right. Note that in many states, the FN-FN blocks share patterning with the clusters obtained using just functional networks, as in the dFNC Cluster Centroids figure below and Demaraju et al (2016). For example FN-FN in ({SFdC states}, dFNC state) as follows are very similar: ({2},I); ({6,10},2) ({3,5},3); ({7,9},4). In particular, for SFdC state 10 which is significantly more occupied by SZ patients, the FN-FN block exhibits the modular pattern of strong intra-sensory connectivity and strong negative coupling between sensory and both cognitive control and

4. DISCUSSION

We present here preliminary evidence that analyses based on hyperlocal measures of fMRI spatial dynamics, including patterns of directional propagation strength (Figure 5, Figure 6, Figure 7) and directionless spatial propagation force (Figure 8, Figure 9) that distribute in structured ways over the brain, differentially for schizophrenia patients and controls. We find that decomposition of spatial propagation

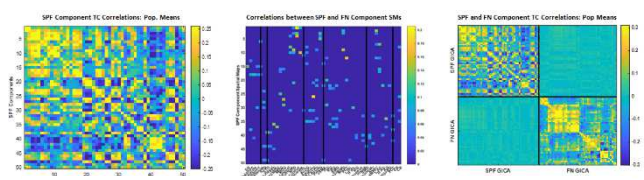


Figure 6 SPF and FN GICAs (Left) Correlations between the 50 SPF GICA component subject-specific TCs: averaged over all subjects; (Middle) Similarity, measured via correlation, between SPF group-level component spatial maps and the FN group-level component spatial maps. The 95th percentile bound on correlation between SPF and FN maps is 0.04; the largest correlation is 0.2. The GICA decompositions based on SPFs and FNs result in very different spatial mappings of the brain. (Right: esp. note off-diagonal blocks) Moreover, the relationship between the temporal contributions of SPF spatial maps to SPF data and the temporal contributions of FN spatial maps to preprocessed fMRI data are also almost entirely uncorrelated. Taken together these results suggest that the spatiotemporal principles governing of localized directional flow strengths and large-scale functional integration are fundamentally different.

force into independent components creates a representation of the brain that is highly independent of the standard

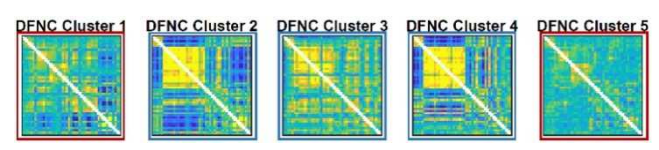


Figure 7 dFNC Cluster Centroids from published work (Damaraju et al (2016)) on this dataset. The FN-FN connectivity, i.e. functional connectivity is in the lower right block of the hybrid SPdC states shown

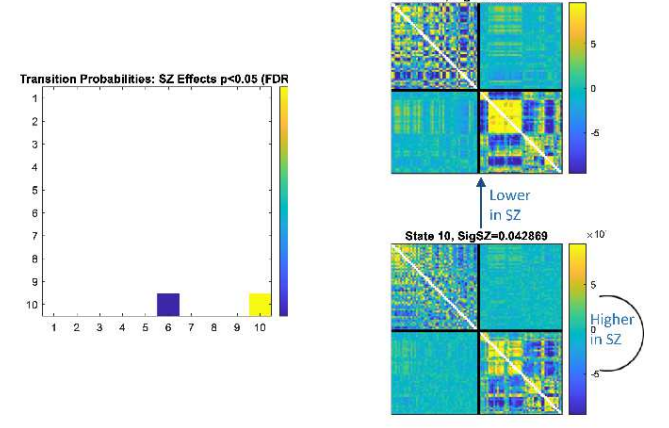


Figure 8 SFdC Transition Probabilities The transition probabilities most significantly mediated by SZ diagnosis (left) involve the two SFdCs whose FN-FN blocks most resemble HC-dominant dFNC cluster 2. SZs are much more likely to stay in SFdC state 10 than HCs, possibly based on the underlying SPF conditions, and SZs are less likely to transition from SFdC state 10 to SFdC state 6 than HCs.

decomposition of preprocessed fMRI into functional networks (**Figure 11**). Evaluating correlations between SPF GICA and FN GICA timecourses concurrently on sliding windows through the scan (Figure 4, Figure 10) paradoxically suggests that the transient patterns of integrative concurrency manifesting jointly over these very different ways of organizing brain space and time can help produce a dynamic characterization of the brain that provides new insights into the base spatial conditions that support large scale patterns of functional integration, and can function as a novel biomarker differentiating schizophrenia patients from controls.

5. ACKNOWLEDGEMENTS

This work was supported by NIH R01MH123610 and NSF 2112455.

6. REFERENCES

- 1. Preti, M.G., T.A. Bolton, and D. Van De Ville, *The dynamic functional connectome: State-of-the-art and perspectives.* Neuroimage, 2017. **160**: p. 41-54.
- 2. Hutchison, R.M., et al., *Dynamic functional connectivity: promise, issues, and interpretations.* Neuroimage, 2013. **80**: p. 360-78.
- 3. Calhoun, V.D., et al., *The chronnectome: time-varying connectivity networks as the next frontier in fMRI data discovery.* Neuron, 2014. **84**(2): p. 262-74.
- 4. Damaraju, E., et al., Dynamic functional connectivity analysis reveals transient states of dysconnectivity in schizophrenia. Neuroimage Clin, 2014. 5: p. 298-308.
- 5. Rashid, B., et al., Dynamic connectivity states estimated from resting fMRI Identify differences among Schizophrenia, bipolar disorder, and healthy control subjects. Front Hum Neurosci, 2014. 8: p. 897.
- 6. Damaraju, E., et al., Dynamic functional connectivity analysis reveals transient states of dysconnectivity in schizophrenia. NeuroImage: Clinical, 2014. 5: p. 298-308.
 - 7. Allen, E.A., et al., *Tracking whole-brain connectivity dynamics in the resting state*. Cereb Cortex, 2014. **24**(3): p. 663-76.
- 8. Abrol, A., et al., Replicability of time-varying connectivity patterns in large resting state fMRI samples. Neuroimage, 2017. **163**: p. 160-176.